Available online at www.sciencedirect.com
ScienceDirect
Journal of the European Ceramic Society 30 (2010) 1163–1170
www.elsevier.com/locate/jeurceramsoc

Electrophoretic deposition as rapid prototyping method

A. Nold *, J. Zeiner, T. Assion, R. Clasen

Saarland University, Department of Powder Technology, Campus C6 3, 66123 Saarbruecken, Germany

Available online 9 May 2009

Abstract

Electrophoretic deposition is a near-net shaping technique leading to excellent green body properties such as high green density and homogeneous pore size distribution that also affect the features of the sintered sample. It has been used in a wide range of applications from optical to biomedical ones. However, it was used as standardized method so that individually tailored geometries have not been fabricated yet. The present work modifies this promising method so that a rapid prototyping process is possible. First of all, the local application of an electric field was investigated and simulated in order to achieve a structure as fine as possible using commercially available coaxial cable. Afterwards, two different ways of fabricating prototype structures with optimized parameters were investigated. The first one was the combination of the developed electrode with a CAM unit. The second one was arranging 16 independent electrodes in a 4 × 4 array in order to parallelize deposition. In all cases, structural integrity as well as height distribution and shape were studied.

Keywords: Shaping; Electrophoretic deposition; Porosity; SiO_2; Rapid prototyping

1. Introduction

Rapid prototyping (RP) methods were developed some years ago in order to fabricate prototypes or only a small number of objects.[1,2] They are classified into additive, subtractive and formative methods. An example for the latter one is nanoprinting.[3] Additive RP means that an arbitrary geometry is built layer-by-layer. Examples are selective laser sintering (SLS)[4] for ceramics or selective laser melting (SLM)[5] for metals. For both processes, the basic material is powder. In case of a metal it is locally melted with a laser, so that hardening occurs. For ceramic systems, either a sintering process takes place or aluminum powder acts as metal binder that is oxidized during sintering.[6] Both methods are nowadays used for fabricating microstructures[7] or for manufacturing composites.[8] A similar RP technique is stereolithography (SL).[9] However, the basic material is a suspension to which a photopolymer is added. The part of the suspension that is irradiated by the laser polymerizes and acts as binder. After finishing the process, the fabricated part needs to be debindered and sintered. This method was applied successfully to fabricate zirconia toughened alumina[10] and for microstructuring.[11]

Inkjet printing as layer-by-layer process also became more and more important in the last years since a modification, the so-called 3D printing,[12] was developed. This method is based on classical inkjet technology whereas an arbitrary structure is built layer-by-layer. It is used for ceramic system based on powder technology. The print head injects a binder so that the powder hardens locally. As a final step, the structure is sintered after debindering. This method was applied successfully to fabricate implants[13,14] and structural ceramic components.[15] Nevertheless, there is still some potential to improve this method.[16] Some other, less known or recently developed RP methods are fused deposition modeling (FDM) that is used for 3D photonic band gap structures[17] or layer-wise slurry deposition (LSD) for fabricating complex shaped ceramics.[18]

Subtractive RP methods start with a bulk material that is removed step by step. Commercially available systems are used in dental industry in order to fabricate individually tailored dental restaurations.[19] Laminated object manufacturing (LOM) however is a mixture between subtractive and additive methods because of its continuous cutting of geometries that are laminated in a second step.[20,21]

Electrophoretic deposition is a suspension-based process for shaping ceramics. It is based on the motion of electrically charged particles in an electric field.[22–25] An advantage compared to other shaping methods such as slip casting or centrifugal casting is the independence of particle velocity from its size.[26] It was successfully applied to fabricate coatings,[27,28] functionally graded materials,[29,30] composite structures[31] and compacts of nanotubes.[32] However, organic suspensions were used and

* Corresponding author.
E-mail address: a.nold@nanotech.uni-saarland.de (A. Nold).

0955-2219/$ – see front matter © 2009 Elsevier Ltd. All rights reserved.
doi:10.1016/j.jeurceramsoc.2009.03.021

special precautions had to be taken. As a result, the presented applications were lab-scale experiments.

A more environmental-friendly approach is to use aqueous suspensions. With water the highest green densities can be achieved and the deposition rate is increased due to the high permittivity of water. As voltages above the decomposition voltage of water have to be applied, problems arise with the formation of gas bubbles at the electrodes. Compared to classical EPD from organic suspensions, it cannot be deposited on the electrodes. Therefore, three different solutions were suggested.[33] First of all, a zinc electrode can be used. In this case, Zn^{2+} is formed instead of bubbles. This was industrially realized with the ELEPHANT process.[34] Secondly, bromide–bromate transition using an electrolyte oxidation might have the same effect. However, high-purity materials cannot be shaped by this modification. The third one is EPD membrane method where the cell in which EPD is carried out is subdivided into 2 chambers by an ion-permeable membrane.[35] The deposition takes place on the membrane so that gas formation and forming of green body are locally separate. This setup was successfully used to fabricate high-purity silica crucibles whereas both the high deposition rate as well as the purity were outlined.[36,37] It was also shown that dental ceramics made from zirconia were fabricated by this method.[38] In this case, expansion gypsum was used as membrane system to compensate sintering shrinkage. The high green density and the possibility to use powder mixtures from nano- and microsized powder to improve mechanical properties were emphasized. Furthermore, optoceramics were fabricated by EPD because of its optimum properties to shape nanosized powder building the base for these ceramic materials.[39–41] These materials are used in microsystem technology such as high-refractive lenses for cameras in cellular phones.

Another advantage of membrane method is the possibility to use a structured membrane that is fabricated by a casting process.[42] In this work, copies of a Euro coin made from nanosized silica powder are presented. Apart from these geometrical parameters, the chemical composition of EPD during deposition can be optimized. This modification is called reactive electrophoretic deposition (REPD). It is based on the manipulation of ion double layer in order to incorporate doping ions into the green body. By doing so, a homogeneous distribution is realized. This method was used to fabricate ruby red glasses[43] as well as coloring glass by incorporating Co^{2+}-ions into the sample.[44]

Apart from the wide range of applications, the green bodies are characterized by its homogeneous pore size distribution[45] as well as the high green density and its homogeneous distribution.[46] As a matter of fact, these properties in combination with the opportunities EPD offer the development of EPD as additive rapid prototyping method is a logical step. Therefore a method was developed, where the deposition is limited to a small spot. Furthermore, it was the objective to get a more homogeneous deposition in comparison to classical RP methods with a layer-wise structuring. This layered structure limits the mechanical properties. A local deposition requires a concentrated electric field, which is a problem in an electrically conducting suspension and needs a special design of the electrodes. A first introduction to this subject with theoretical predictions of electric field distribution simulations was given in Ref.[47] Here this method was applied to the construction of point electrodes.

2. Experimental setup

The powder used was nanoscaled fumed silica powder Evonik Degussa OX50 with a mean particle size of 40 nm and a specific BET surface area of 50 m^2/g. The suspensions were prepared by stirring OX50 into purified water and a solid content of 40 wt.% was achieved. The pH was adjusted to 12 by adding tetramethylammoniumhydroxide (TMAH). The suspension composition was kept constant for all experiments.

Electrophoretic deposition was carried out according to the membrane method in a cell as shown in Fig. 1. Two cathodes and two anodes were mounted whereas the major ones controlled the deposition. The membrane was prepared from a solution consisting of 30 parts poly(methyl methacrylate), 6 parts MMA (methyl methacrylate), 3 parts Tergitol NP-9 and 12 parts bidistilled water. The membrane was formed by pouring the solution in a mold with the desired form. Afterwards, the solid membrane was immersed in the electrolyte and left there to soak. The electrolyte in the compensation chamber had an electric conductivity that was 10 times that of the suspension. Thus the counter electrodes reduced deposition caused by the concentration gradient between both chambers. The suspension chamber had a length of 30 mm and the compensation chamber 22.5 mm. In order to investigate the possibility to apply an electric field locally, spot-wise deposits were fabricated whereas parameters such as applied voltage U and deposition time t were varied. The used electrodes were modified coaxial cables with an inner copper core and a shielding to focus the electric field. The dimensions of the major electrodes are shown in Fig. 2. The experiments were performed with the coaxial-cables-shield ground potential. The copper core and shielding at the outer edge were both either 1 mm retracted from the electrode end or not retracted at all. These electrodes were controlled by a CAM unit RoboMate 600i (FANUC Inc., Japan).

The electrical field distribution between the major coaxial-cable electrodes was simulated through finite element analysis with the FlexPDE program. The generated mesh of the longi-

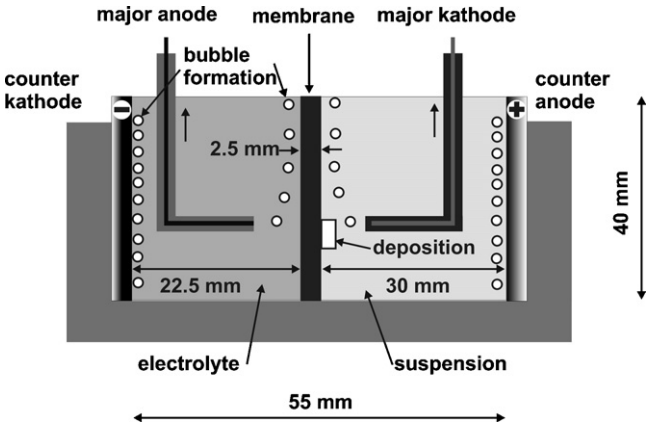

Fig. 1. EPD cell, major anode and cathode were moved by the CAM unit.

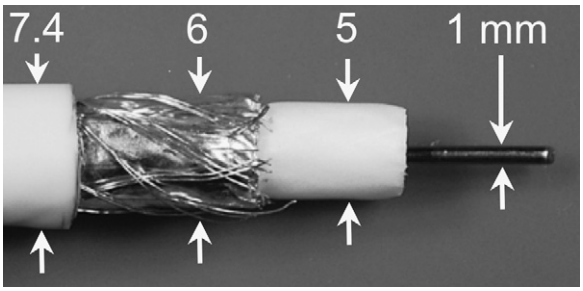

Fig. 2. Relative dimensions of the major anode (and cathode) employed in the experimental setup shown in Fig. 1.

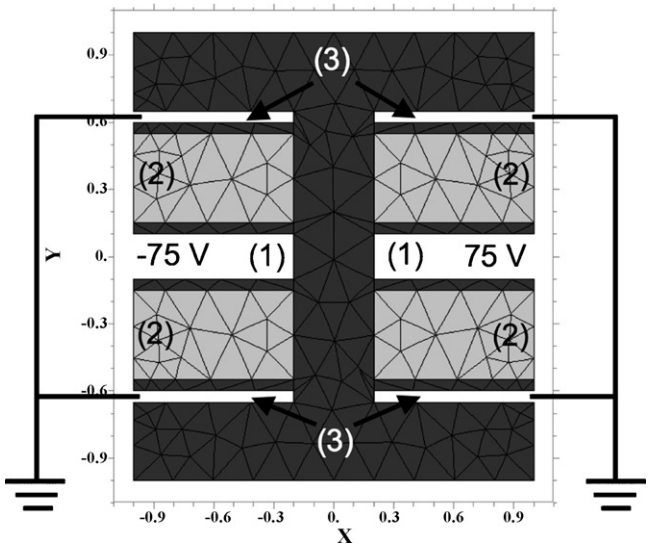

Fig. 3. Generated mesh of the longitudinal cut of both coaxial electrodes. (1) Metallic core, (2) insulating material, (3) metallic shielding, which can be grounded.

tudinal cut of both coaxial electrodes is presented in Fig. 3. A voltage of 150 V was applied between the electrodes. In order to fabricate prototype structures such as lines with a length of 1 cm and perpendicular lines with a basis length of 1 cm. Motion speed was between 1 and 1.33 cm/min.

The developed electrode array is presented in Fig. 4a. The electrode dimensions are shown in Fig. 5. The electrodes are twice smaller than the ones used with the CAM unit and the distance between two inner cores is 4.5 mm in each direction. They can be switched on and off separately according to the

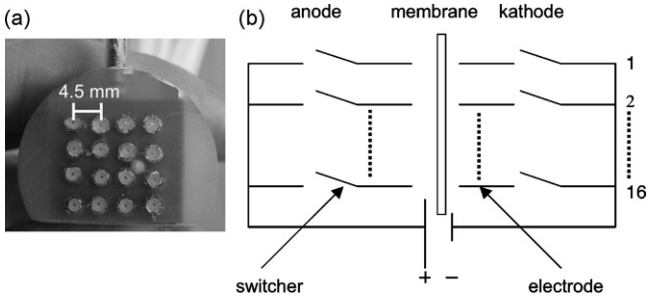

Fig. 4. (a) 4 × 4 array consisting of 16 independently switchable electrodes as shown in (b).

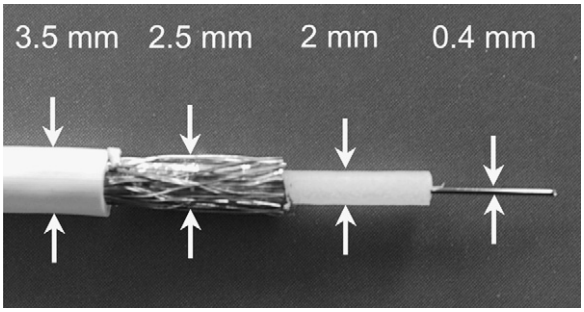

Fig. 5. Relative dimensions of the switchable electrodes employed in the experimental setup shown in setup of Fig. 4.

simplified circuit diagram in Fig. 4b. In some experiments, a counter voltage was applied to the shielding of deposition and counter electrode in order to study if the spot-wise deposits can be reduced in diameter. Furthermore, there were two distances d_1 and d_2, whereas d_1 was the one between array and membrane in the suspension and d_2 the one between membrane and array in the compensation chamber. The height profile of the deposits (green bodies) was determined using a Denta-Scope scanner with the software ScanOS (BEGO Bremer Goldschlaegerei, Germany).

3. Results and discussion

3.1. CAM approach

The results for the non-retracted copper-core experiments are shown in Fig. 6. A significant influence of applied voltage is found if deposition time is kept constant. Increasing U by factor two leads to different shapes and sizes. For 100 V, a disc shape is found with a maximum height in the middle of the green body as visible in Fig. 6b. For 200 V, the shape remains the same even if the maximum in height is not found in the middle any longer. For this case given in Fig. 6a, ascending bubbles were stopped by the deposit growth and included into the green body leading to defects. Fig. 6c shows the result if deposition time is decreased from 4 min to 30 s while keeping U constant at 200 V. This image confirms the aforementioned explanation for this case, where the growth of the deposit was less fast so that the bubbles were

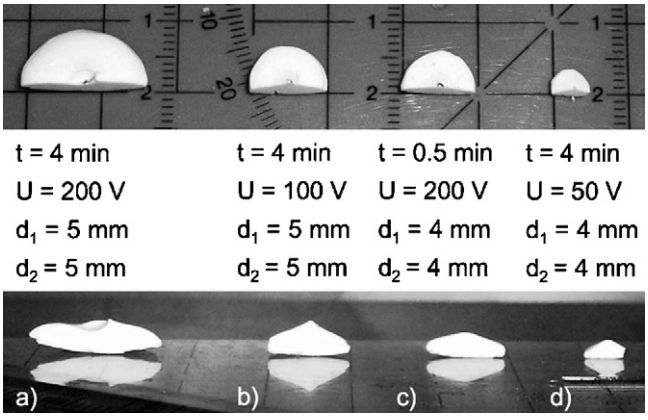

Fig. 6. Fabricated spot-wise deposits by locally applying an electric field.

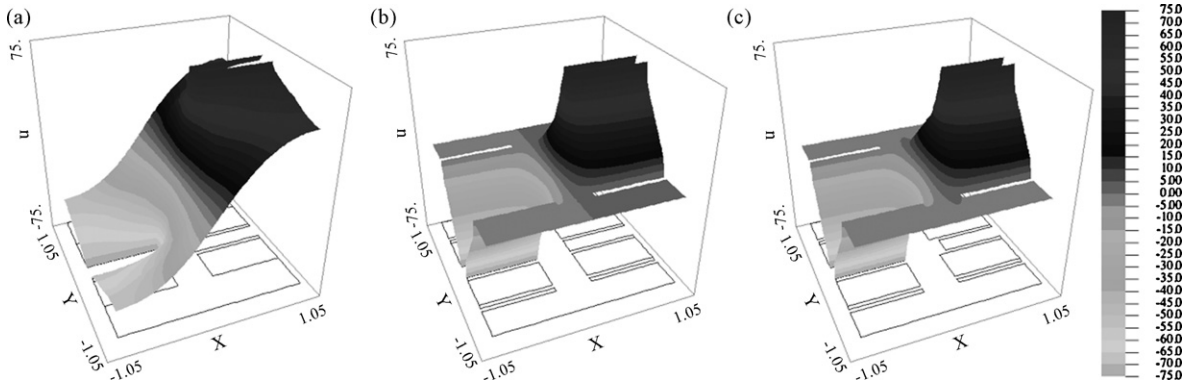

Fig. 7. Potential distribution between two coaxial cable electrodes. (a) No metallic shielding available and cable core is not retracted. (b) Metallic shielding available and grounded, core is not retracted. (c) Metallic shielding grounded and cable core retracted.

not included. Furthermore, the diameter is about the same as in Fig. 6b whereas the maximum in height is less distinct. A final result is given in Fig. 6d. Here, $t = 4$ min and $U = 50$ V were the deposition parameters. The shape is still disc-like. However, both diameter and height are smaller. With this investigation, the influence of different parameters was shown. It was found that high voltages combined with small deposition times lead to similar results as small voltages with high deposition times. However, a growth in diameter with time and applied voltage was also investigated. With increasing time, diameter growth is much faster than height growth. At a certain point, the latter is limited by bubble formation leading to big pores inside the sample.

The simulated electric field distributions are shown in Fig. 7. The first simulations were performed with the coaxial-cables-shield ungrounded (a), afterwards the cables shields were grounded (b) and finally the copper core was 1 mm inside the insulating material retracted (c). The borders projected on the bottom plane of Fig. 7a, b and c show the configuration of each electrode setup employed. The results show how the electric field lines propagate widely outside the electrode surfaces when no shielding is employed (Fig. 7a). As the electric field is not focused, only point deposits with relatively larger diameter can be obtained. By grounding the electrode shielding, the focalization of the electric field becomes stronger. This effect is observed in Fig. 7b, where less changes appear on the edges of the surface representing the simulated potential distribution. By retracting the copper core (and keeping the shielding grounded), the change on the potential-distribution-surface edges of Fig. 7c disappears. That is, the electric field is well-focused and therefore successfully suppressed at the electrode edges.

The simulation results were experimentally controlled as shown in Figs. 8 and 9. Point deposits were produced under a voltage of 100 V and the deposition time was varied. One of the experiment series was performed with coaxial-electrodes-shield grounding only; the other one was performed with shields grounding and also the depositing electrode copper core was 1 mm retracted. It is clear that the latter case point deposits were around 2 times smaller in heights and diameters. These experimental results confirm the behavior expected according to the simulations performed.

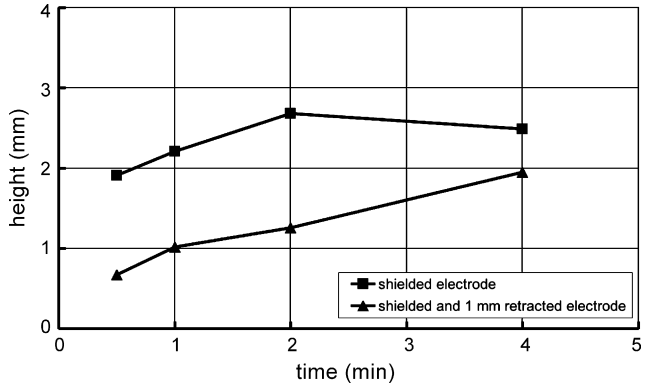

Fig. 8. Point deposit height as function of deposition time. Deposition voltage = 100 V.

Fig. 10 shows two samples prepared with the same motion velocities and the same distances, $d_1 = d_2 = 2$ mm, but different applied voltage. The length of the path to be gone was 1 cm in each case whereas the applied voltages were different with 100 V (Fig. 10a) and 200 V (Fig. 10b). In Fig. 10a, the final length and width are 11.5 and 6.4 mm respectively. However, height distribution is much more important. Its homogeneity becomes evident by the grey surface representing the highest part. Furthermore, it can be observed that height decreases down to zero along

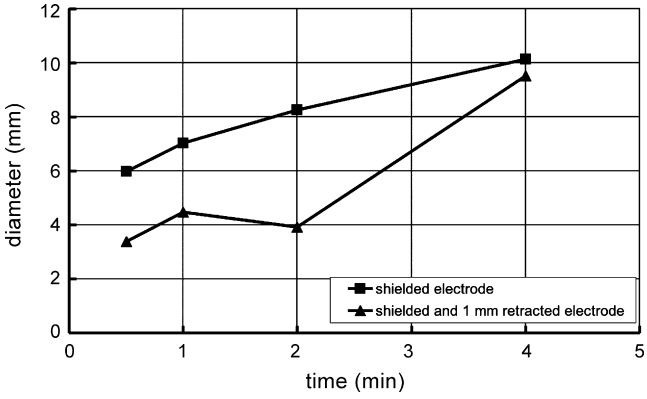

Fig. 9. Point deposit diameter as function of deposition time. Deposition voltage = 100 V.

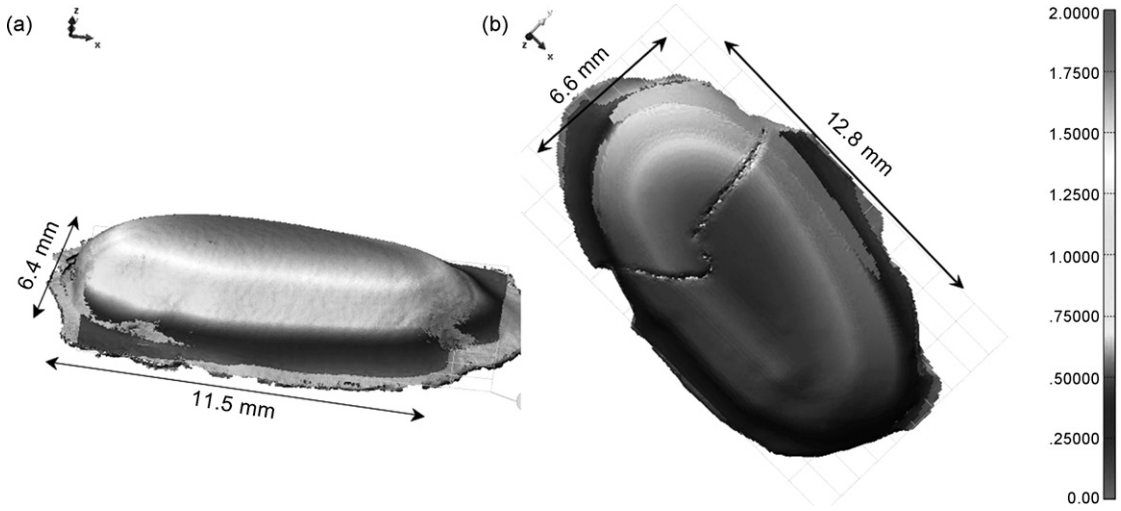

Fig. 10. (a) Line deposits, fabricated with $U = 100$ V and $v = 1.0$ cm/min, b) $U = 200$ V and $v = 1.0$ cm/min.

all sides. This decrease is also homogeneous. The grey parts of the sample could not be scanned. For the sample shown in 10b, motion velocity was also 1.0 mm/min but the applied voltage was 200 V. Its width is 6.6 mm and length 12.8 mm. Again, a similar homogeneity is found with a maximum in height in the middle of the top surface whereas height decreases to the edges as seen before. The visible crack occurred while preparing the sample for the 3D scan and is therefore not caused by the process. Apart from the height profile, microstructural homogeneity was confirmed by SEM investigations. No lamination or shell-like structures were found in the EPD samples.

As the used CAM unit offers two control modes, joint and linear , their influence on deposit geometry was also studied. The result is given in Fig. 11 where two perpendicular lines were fabricated staring in point 1, moving over 2 where the mode was changed from joint to linear. The end of deposition was in point 3. The better mode for RP-EPD is obviously linear because of the homogeneous height profile. For linear moving, motion tolerances are increased so that the electrodes are sometimes closer to the membrane and sometimes further away. Thus the distance is not supposed to be constant at all the times. In the starting point 1, the best height is located due to the beginning motion. Along the first leg, an inhomogeneous height distribution is found. This is as aforementioned caused by the increased tolerance values for the motion.

3.2. Array approach

Using an array consisting of 4×4 electrodes represents an alternative to the presented CAM controlled motion. In this case,

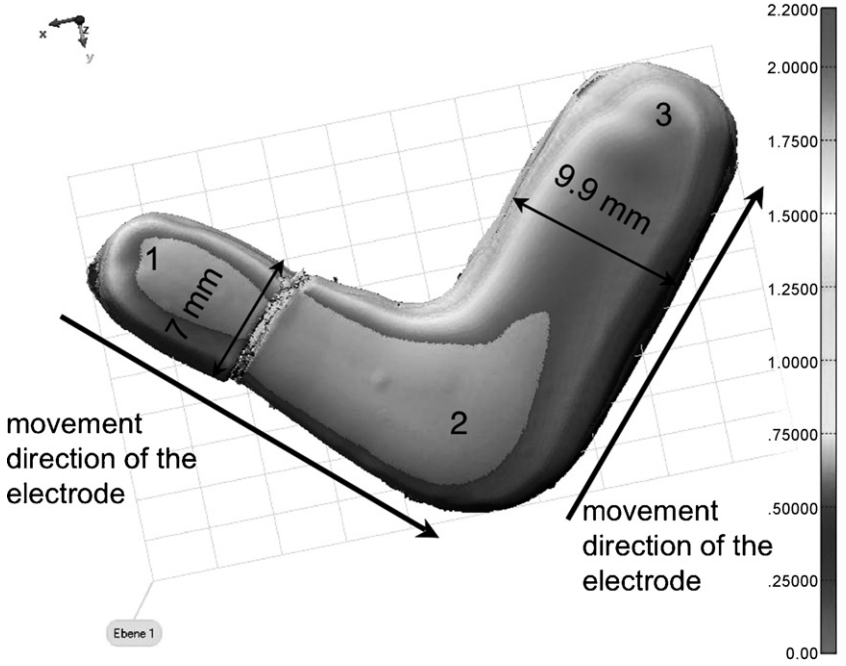

Fig. 11. Perpendicular lines, fabricated by motion of CAM unit in two different modes (joint and linear).

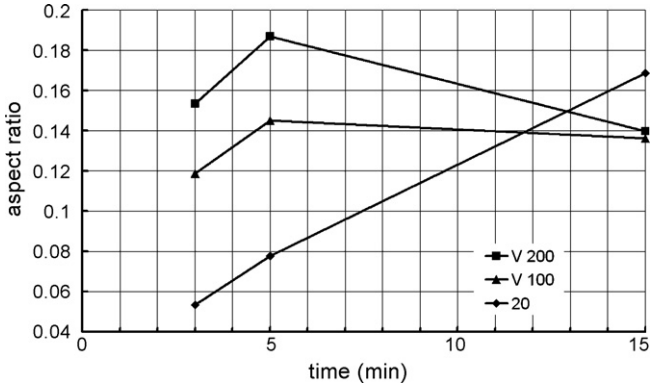

Fig. 12. Aspect ratios for $d_1 = 3$ mm and $d_2 = 2$ mm for different applied voltages as function of deposition time.

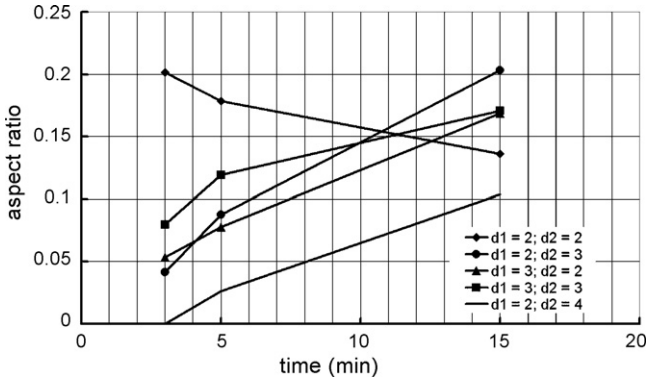

Fig. 13. Aspect ratios for $U = 20$ V for different array distances as function of deposition time.

the shape of spot-wise deposits was the same as for the electrode used in the CAM approach. However, for this investigation, both the evolution of aspect ratio (ratio of height and width, in this case diameter) for different applied voltages at constant distance d between the arrays in both chambers as well as constant voltage for different distances d were studied. Fig. 12 presents the achieved aspect ratio for constant voltages of 20, 100 and 200 V for different deposition times t ranging between 3 and 15 min. Only for the smallest investigated voltage of 20 V, a linear increase in aspect ratio is found. For the last two, 100 and 200 V, a maximum at 5 min is observed. It is between 0.14 and 0.18. However, it decreases to a constant value of about 0.137 after 15 min for both applied voltages. In contradiction to this result, an aspect ratio of 0.17 is found for 20 V. This example clarifies the influence of deposition time and applied voltage. From a certain time on – in the present case for $t > 5$ min – the deposit grows faster in diameter than in height so that the aspect ratio decreases. This is due to the fact that a growing deposit weakens the electric field so that new particles are rather accumulated at the edges than at the top. As a result, an optimum time for an optimized aspect ratio exists.

Compared to the result just presented, the influence of different distances between the electrodes is also an important factor that needs to be taken into account if applying EPD as RP method. The results of this study are given in Fig. 13 for a constant major voltage of 20 V.

Fig. 14 shows the results of the fabricated letters "L", "P" and "T". In (a), both the single dots looking similar to the spot-wise deposits as well as the position of the electrodes during deposition can be easily recognized. There is a small distance between them so that the resolution limit has not been reached yet. In Fig. 14b, a "P" structure was fabricated. Here, the problem to be investigated was the closed structure in the middle. Again, it is clearly recognizable whereas the distances between single dots disappeared and overlapped. Nevertheless, the position of the deposition electrodes can still be found. Moreover, it became evident that inclusion of bubbles in the middle of "P" is avoided by this optimum choice of deposition parameters. A less optimum set of parameters is presented in Fig. 14c. The letter "T" shows defects and channels where the bubbles were drained. This structure was deposited upside-down in order to reduce structural impurities caused by bubble formation.

In order to focus the field even more than in these experiments, a counter voltage was applied to the shielding. Fig. 15 shows the aspect ratios (height/diameter) of spot-wise deposits that were prepared by applying different counter voltages to the

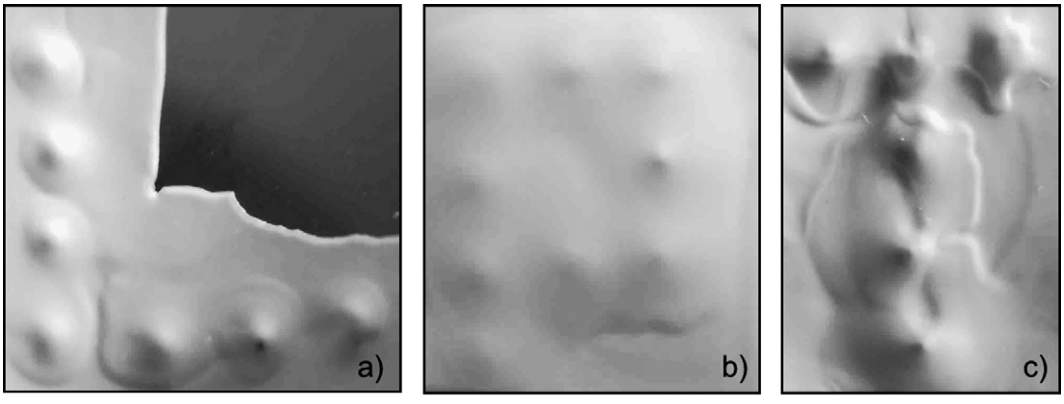

Fig. 14. Prototype structures fabricated using the 4 × 4 array: (a) letter L, (b) letter P and (c) letter T.

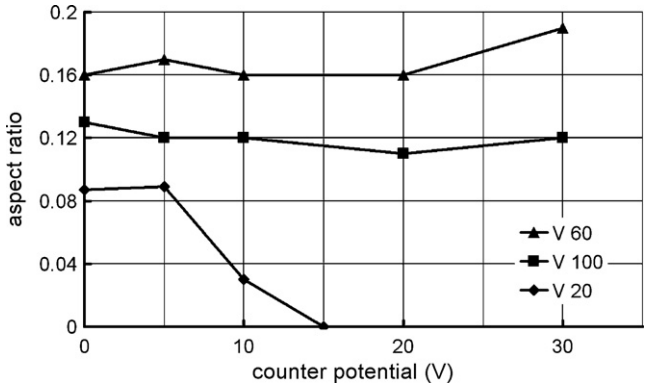

Fig. 15. Aspect ratio of spot-wise deposits as function of applied counter field at the shielding.

shielding. For a major electric field of 20 V, the aspect ratio remains constant until a counter voltage of 5 V. Increasing it to 10 V decreases the aspect ratio by factor 2 whereas no deposition was found for values larger than 10 V. For an applied voltage of 100 V, all aspect ratios remain constant at about 0.12 for counter voltages between 0 and 30 V. Larger counter fields were not studied because of an increasing deposition on the counter electrode. A constant value of 0.16 is found for a major voltage of 60 V for all applied counter voltages whereas values larger than 30 V were not investigated for aforementioned reasons. As a result, it was found that the use of counter voltages does not lead to the effect that was expected. The shape of the deposits was modified but a decrease in diameter was not observed.

4. Conclusions

The present work introduced EPD as rapid prototyping method. Two approaches were chosen whereas the first one was the use of a shielded electrode that was combined with a translational motion. The second one was a parallelization of the first one by developing an electrode array consisting of 4×4 shielded electrodes.

First of all, spot-wise deposits were fabricated to study the localization of the electric field in the CAM approach. A small electric field (=applied voltage) combined with an optimized deposition time led to the best results. Furthermore, prototype structures such as lines and letters were fabricated. For the line made using the CAM unit, a homogeneous height distribution was observed. The formation of layers or a shell-like microstructure did not occur. The letters "L", "P" and "T" were deposited using the array approach. In this case, both the asymmetric distance between the array in the suspension and compensation chamber as well as the process time t and applied voltage U mainly influenced the structural integrity. The position of the electrode was recognized in the fabricated samples due to the peaks in height. Furthermore, the structure limits of the array process have not yet been found. The resolution will be enhanced in future work.

As a final conclusion, the high potential of EPD as RP method was emphasized whereas further developments are still necessary. Especially the size of the structures needs to be downscaled.

Acknowledgements

The authors would like to thank to the German Research Foundation (DFG) for their support of this work under grant number CL 102/25-1.

The support of Dr. Stephan Dierkes and Jan Eilers (BEGO Dental Systems, Bremen, Germany) for their support determining the height profiles of the samples is also gratefully acknowledged.

References

1. Edirisinghe, M. J., In *Solid Freeform Fabrication of Ceramics. In Processing and Fabrication of Advanced Materials VII*, ed. T. S. Srivatsan and K. A. Khor. The Minerals, Metals & Materials Society, 1998, pp. 139–149.
2. Hopkinson, N. and Dickens, P., Rapid prototyping for direct manufacture. *Rapid Prototyping J.*, 2001, **7**, 197–202.
3. Yokoo, A., Nakao, M., Masuda, H. and Tamamura, T., Direct nanoprinting technology and its application to nanostructure fabrication. *LEOS*, 2000, **2**, 417–418.
4. Tay, B. Y., Evans, J. R. G. and Edirisinghe, M. J., Solid freeform fabrication of ceramics. *Int. Mater. Rev.*, 2003, **48**, 341–370.
5. Bourell, D. L., Marcus, H. L., Barlow, J. W. and Beaman, J. J., Selective laser sintering of metals and ceramics. *Int. J. Powder Metall.*, 1992, **28**, 369–381.
6. Subramanian, P. K. and Marcus, H. L., Selective laser sintering of alumina using aluminium binder. *Mater. Manuf. Processes*, 1995, **10**, 689–706.
7. Kathuria, Y. P., Microstructuring by selective laser sintering of metallic powder. *Surf. Coat. Technol.*, 1999, **116–119**, 643–647.
8. Lorrison, J. C., Dalgarno, K. W. and Wood, D. J., Processing of an apatite-mullite glass-ceramic and an hydroxyapatite/phosphate glass composite by selective laser sintering. *J. Mater. Sci.: Mater. Med.*, 2005, **16**, 775–781.
9. Griffith, M. L. and Halloran, J. W., Freeform fabrication of ceramics via stereolithography. *J. Am. Ceram. Soc.*, 1996, **79**, 2601–2608.
10. Licciulli, A., Corcione, C. E., Greco, A., Amicarelli, V. and Maffezzoli, A., Laser stereolithography of ZrO_2 toughened Al_2O_3. *J. Eur. Ceram. Soc.*, 2005, **25**, 1581–1589.
11. Bertsch, A., Jiguet, S. and Renaud, R., Microfabrication of ceramic components by microstereolithography. *J. Micromech. Microeng.*, 2004, **14**, 197–203.
12. Sachs, E. M., Haggerty, J., Cima, M. J. and Paul, P., Three-dimensional printing techniques. US 5,204,055 (1993).
13. Curodeau, A., Sachs, E. and Caldarise, S., Design and fabrication of cast orthopedic implants with freeform surface textures from 3D printed ceramic shell. *J. Biomed. Mater. Res.*, 2000, **53**, 525–535.
14. Webb, P. A., A review of rapid prototyping (RP) techniques in the medical and biomedical sector. *J. Med. Eng. Technol.*, 2000, **24**, 149–153.
15. Cima, M. J., Yoo, J., Rynerson, M., Nammour, D., Giritlioglu, B., Grau, J. and Sachs, E. M., Structural ceramic components by 3D printing. In *Proceedings of the Symposium on Solid Freeform Fabrication*, 1995, pp. 479–488.
16. Sachs, E. and Vezzetti, E., Numerical simulation of deposition process for a new 3DP printhead design. *J. Mater. Process. Technol.*, 2005, **161**, 509–515.
17. Pilleux, M. E., Allahverdi, M., Chen, Y., Lu, Y., Safari, M. A. and Safari, A., 3D photonic bandgap structures in the microwave regime by fused deposition of multimaterials. *Rapid Prototyping J.*, 2002, **8**, 46–52.
18. Günster, J., Engler, S. and Heinrich, J. G., Forming of complex shaped ceramic products via laser-wise slurry deposition (LSD). *Bull. ECerS*, 2003, **1**, 25–28.
19. Willer, J., Rossbach, A. and Weber, H.-P., Computer-assisted milling of dental restorations using a new CAD/CAM data acquisition system. *J. Prosthet. Dent.*, 1998, **80**, 346–353.
20. Cawley, J. D., Heuer, A. H., Newman, W. S. and Mathewson, B. B., Computer-aided manufacturing of laminated engineering materials. *Am. Ceram. Soc. Bull.*, 1996, **75**, 75–79.
21. Crawley, J. D., Computer-aided manufacturing of laminated engineering materials (CAM-LEM) and its application to the fabrication of ceramic

components without tooling. *In International Gas Turbine & Aeroengine Congress & Exhibition*. The American Society of Mechanical Engineers, Orlando, FL, 1997 [Paper 97-GT-534].
22. Fukada, Y., Nagarajan, N., Mekky, W., Bao, Y., Kim, H.-S. and Nicholson, P. S., Electrophoretic deposition—mechanisms, myths and materials. *J. Mater. Sci.*, 2004, **39**, 787–801.
23. Clasen, R. and Tabellion, J., Electric-field-assisted processing of ceramics. Part I. Perspectives and applications. *cfi/Ber. DKG*, 2003, **80**, E40–E45.
24. Oetzel, C., Clasen, R. and Tabellion, J., Electric-field assisted processing of ceramics. Part II. Electrophoretic impregnation and use for manufacturing of glass and ceramic functionally graded materials. *cfi/Ber. DKG*, 2004, **81**, E35–E41.
25. Besra, L. and Liu, M., A review on fundamentals and applications of electrophoretic deposition (EPD). *Prog. Mater. Sci.*, 2007, **20**, 1–61.
26. Hamaker, H. C., Formation of a deposit by electrophoresis. *Trans. Faraday Soc.*, 1940, **36**, 279–287.
27. Put, S., Vleugels, J., Anné, G. and Biest, O. V. d., Processing of hardmetal coatings on steel substrates. *Electrophoretic Deposition: Fundamentals and Applications*. The Electrochemical Society, Inc., 2002, pp. 183–190.
28. Biest, O. V. d., Joos, E., Vleugels, J. and Baufeld, B., Electrophoretic deposition of zirconia layers for thermal barrier coatings. *J. Mater. Sci.*, 2006, **41**, 8086–8092.
29. Vandeperre, L. J. and Biest, O. O. v. d., Graceful failure of laminated ceramic tubes produced by electrophoretic deposition. *J. Eur. Ceram. Soc.*, 1998, **18**, 1915–1921.
30. Put, S., Vleugels, J. and Biest, O. V. d., Functionally graded WC–Co materials produced by electrophoretic deposition. *Scripta Mater.*, 2001, **45**, 1139–1145.
31. Put, S., Anné, G., Vleugels, J. and Biest, O. V. d., Functionally graded ZrO_2–WC composites processed by electrophoretic deposition. *Key Eng. Mater.*, 2002, **206-213**, 189–192.
32. Boccaccini, A. R., Cho, J., Roether, J. A., Thomas, B. J. C., Minary, E. J. and Shaffer, M. S. P., Electrophoretic deposition of carbon nanotubes. *Carbon*, 2006, **44**, 3149–3160.
33. Clasen, R., Preparation of very pure silica glasses by sintering submicron particles (in German). Thesis for an appointment of an university lectureship, Aachen University of Technology, Aachen, 1989.
34. Chronberg, M. S. and Händle, F., Processes and equipment for the production of materials by electrophoresis ELEPHANT. *Interceramics*, 1978, **27**, 33–34.
35. Clasen, R., Forming of compacts of submicron silica particles by electrophoretic deposition. In *In 2nd International Conference on Powder Processing Science*, ed. H. Hausner, G. L. Messing and S. Hirano, 1988, pp. 633–640, 12–14. 10. 1988.
36. Tabellion, J., Clasen, R. and Schwertfeger, F., Elektrophoretisch nachverdichtete SiO_2-Formkörper, Verfahren zu ihrer Herstellung und Verwertung. DE 10044163A1, 2000.
37. Günster, J., Engler, S., Heinrich, H. J. and Schwertfeger, F., A novel route for the production of ultrapure SiO_2 crucibles. *Glass Sci. Technol.*, 2005, **78**, 18–22.
38. Oetzel, C. and Clasen, R., Preparation of zirconia dental crowns via electrophoretic deposition. *J. Mater. Sci.*, 2006, **41**, 8130–8137.
39. Braun, A., Falk, G. and Clasen, R., Transparent Polycrystalline alumina ceramic with sub-micrometre microstructure by means of electrophoretic deposition. *cfi/Ber. DKG*, 2005, **82**, 162–165.
40. Wolff, M., Braun, A., Bartscherer, E. and Clasen, R., Preparation of polycrystalline ceramic compacts made of alumina powder with a bimodal particle size distribution for hot isostatic pressing. *Ceram. Eng. Sci. Proc.*, 2003, **24**, 81–86.
41. Wolff, M. and Clasen, R., Fabrication of transparent polycrystalline zirconia ceramics. *cfi/Ber, DKG*, 2005, **82**, E49.
42. Zeiner, J. and Clasen, R., Fabrication of microstructures by means of electrophoretic deposition (EPD). *Key Eng. Mat.*, 2006, **314**, 57–62.
43. Tabellion, J., Zeiner, J. and Clasen, R., Manufacturing of pure and doped silica and multicomponent glasses from SiO_2 nanoparticles by reactive electrophoretic deposition. *J. Mater. Sci.*, 2006, **41**, 8173–8180.
44. Jung, D., Tabellion, J. and Clasen, R., Influence of dopants on the suspension properties and reactive electrophoretic deposition. *Key Eng. Mat.*, 2006, **314**, 81–86.
45. Tabellion, J., Clasen, R. and Jungblut, E., Near-shape manufacturing of ceramics and glasses by electrophoretic deposition using nanosized powders. *Ceram. Eng. Sci. Proc.*, 2003, **24**(3).
46. Tabellion, J. and Clasen, R., Near-shape manufacturing of complex silica glasses by electrophoretic deposition of mixtures of nanosized and coarser particles. In *In Ceramic Engineering and Science Proceedings, 28th International Conference on Advanced Ceramics and Composites: B*, ed. E. Lara-Curzio and M. J. Ready, 2004, pp. 585–590.
47. Zeiner, J., Nold, A., Clasen, R. and Electrophoretic, Deposition as shaping technique—a CAM approach. *Adv. Sci. Technol.*, 2006, **45**, 714–719.